JOURNAL OF AIRCRAFT
Vol. 46, No. 1, January–February 2009

Engineering Notes

ENGINEERING NOTES are short manuscripts describing new developments or important results of a preliminary nature. These Notes should not exceed 2500 words (where a figure or table counts as 200 words). Following informal review by the Editors, they may be published within a few months of the date of receipt. Style requirements are the same as for regular contributions (see inside back cover).

Comparison of Conventional and Compression Pylon Designs for an Underwing Nacelle

R. Devine,* R. K. Cooper,† R. Gault,‡ and J. K. Watterson†
Queen's University of Belfast,
Belfast, Ireland BT9 5AH, United Kingdom
and
E. Benard§
University of Glasgow,
Glasgow, Scotland G12 8QQ, United Kingdom

DOI: 10.2514/1.34967

I. Introduction

THE challenge to the aerospace community today is to design and build environmentally friendly aircraft that are both safer and more affordable to own and operate. This paper addresses one of the key components required to produce an environmentally friendly aircraft by reducing drag (and hence fuel consumption) through improved aerodynamic integration of the wing, pylon, and nacelle.

Installation of the pylon and nacelle on a transonic aircraft wing has significant effect on chordwise and spanwise load distributions, shock position, and the viscous layer on the surface, and, therefore, performance. For example, the complexities involved in airframe powerplant integration in relation to the Boeing 777 have been highlighted by Berry [1]. A number of experimental transonic studies related to airframe/propulsion integration have been conducted at NASA on high wing [2] and low wing [3] mounted nacelles. Those investigations have demonstrated that installation of the pylon and nacelle can lead to increases in viscous, interference, and form drag and a loss of total lift. In general the aerodynamic interactions are sensitive to nacelle shape, the bypass ratio, location of the pylon nacelle in relation to the wing, and the nature of the boundary layer on the nacelle, that is, laminar or turbulent [4]. It was recognized that most of the unfavorable effects are caused by the pylon, with little contribution from the nacelle/pylon combination. Exploring the design space, systematic investigations have been performed on the effects of nacelle and pylon location in relation to the wing [5]. One of the main conclusions was that installation drag was most sensitive to the horizontal position of the nacelle, but not very sensitive to its vertical position. The minimum drag was found with the nacelle farthest upstream from the wing as this position minimizes the variation of the cross-sectional area with flow direction, that is, it follows the area rule.

The influence of pylon geometry can be gleaned from the experiments performed at NASA Langley Research Center [6–8] on propulsion integration. The investigations demonstrated the need for a careful contouring of the pylon/wing interface to reduce the adverse installation effects, such as lift loss due to the acceleration of airflow and subsequent shock caused by the presence of the pylon. Carlson and Lamb [9] investigated a compression pylon design on the premise of potentially lower installation drag. This design was subjected to several wind-tunnel tests at NASA Langley Research Center in the late 1980s and compared to several different pylon designs. However, those experiments were conducted without a nacelle attached, and therefore the present work explores the performance of the combination of a nacelle with a compression pylon.

II. Numerical Simulations, Schemes, and Grid

Although there is still an issue with the ability of computational fluid dynamics (CFD) to predict accurately the complex flows associated with the wing-pylon-nacelle interaction, Reynolds averaged Navier–Stokes calculations have demonstrated reasonable accuracy in this regard [10]. The present investigation used a commercial CFD code, FLUENT ™, to model compressible flows around whole body aircraft configurations (excluding fin and tailplane). The numerical model was based on the system of time-dependent Navier–Stokes equations, expressed in conservation form. The solution method used a fully implicit finite volume scheme of second-order accuracy. The solver was run in coupled implicit mode using a Spalart–Allmaras [11] turbulence model, with the Fluent 6 standard model coefficients. This was chosen due to its satisfactory performance in the Second AIAA Drag Prediction Workshop [12]. Flow-through nacelles, without jet simulation, were used in the present investigations as it has been demonstrated that the effects of engine exhaust jet flow on wing-nacelle interactions are negligible [13].

In previous work [14,15], with a medium sized grid (6–11 $\times$ 10^6 points), the accuracies in predicting the drag coefficient of a wing-body configuration due to the grid, the code, the turbulence model, and fixing transition were 5, 5, 7, and 10 drag counts ($\delta C_D = 0.0001$), respectively. The corresponding figures for a wing-body-pylon-nacelle (WBPN) configuration were 11, 10, 15, and 11 drag counts, respectively. The results of the analysis presented here must be viewed in light of these accuracies in prediction.

In the present study, ICEMCFD™ unstructured meshes were used due to the relative automation of mesh generation, compared with structured meshing methods. To meet the mesh requirements for an accurate model using unstructured meshes, a hybrid mesh strategy was put in place. For the initial set of calculations, in which the baseline configuration was studied with and without the pylon nacelle, 30 prismatic layers were grown from the surface mesh at a

Presented as Paper 6340 at the AIAA 4th Aviation Technology, Integration and Operations (ATIO) Forum, Chicago, Illinois, 20–22 September 2004; received 4 October 2007; revision received 15 April 2008; accepted for publication 15 April 2008.

*Research Assistant, Centre Of Excellence In Integrated Aircraft Technologies (CEIAT), School of Mechanical and Aerospace Engineering, Ashby Building, Stranmillis Road. Member AIAA.

†Senior Lecturer, Centre Of Excellence In Integrated Aircraft Technologies (CEIAT), School of Mechanical and Aerospace Engineering.

‡Research Assistant, Centre Of Excellence In Integrated Aircraft Technologies (CEIAT), School of Mechanical and Aerospace Engineering, Ashby Building.

§Senior Lecturer, Department of Aerospace Engineering. Member AIAA.

growth rate of 1.2, with a first cell height set to Y^+ of approximately 1. The computational domain measured $142 \times 142 \times 71$ mean aerodynamic chord lengths. The hybrid mesh consisted of approximately 10×10^6 nodes: this can be classified as medium to fine; similar meshes have demonstrated the potential for accurate predictions [12,16].

The second set of calculations compared the performance of the conventional WBPN with that of a WBPN employing a compression pylon. The choice of flow solver, turbulence model, and meshing technique used for the compression pylon were the same as in the conventional geometry case. However, to obtain a converged solution for the new configuration, it was necessary to create a new mesh with 23 prismatic layers. For comparison purposes the baseline WBPN case was also remeshed with 23 prismatic layers. This meant both meshes had approximately 8×10^6 elements.

III. Configurations

Two configurations were tested in this work. The DLR F6 configuration was tested to validate the CFD techniques. The nacelle is axisymmetric with lines derived from the CFM56-5 nacelle in a long duct version and the original pylon is of symmetrical shape. Extensive wind-tunnel tests of the F6 configuration were conducted in the ONERA S2MA 1.77×1.75 m transonic wind tunnel during the period 1990–1998 [17]. In comparison with similar works at NASA [3], this configuration exhibits a much larger interference effect as there is only a narrow gap between the wing and the nacelle (less than 10% of the local chord).

The second configuration was similar to the first, except the pylon was changed from a conventional design to a compression pylon design (Fig. 1) to reduce the adverse interference of the pylon. Relative maximum thickness was kept close to that of the original pylon to reflect partially some pylon stressing and stiffness constraints.

IV. Results and Discussions

Results presented here are for a Mach number of 0.75 and a Reynolds number, based on the mean aerodynamic chord, of 3×10^6. The transition was fixed on all surfaces by transition strips. The computations overpredict the lift coefficient, at every design point (Fig. 2), by 0.02 to 0.03 for the wing-body (WB) configuration and by 0.03 to 0.04 for the WBNP configuration. These differences for the lift coefficient are slightly higher than the ones ranging from 0.017 to 0.03 for both configurations, obtained in the DLR study [16]. The interpolated angle of attack corresponding to $C_L = 0.5$ was found to be approximately 0.68 deg. This value compares favorably with the average angle of the simulations of the Second AIAA Drag Prediction Workshop [12], $\alpha = 0.72$ deg. The drag coefficients are also overpredicted by 0.004 (WB) and 0.0036 (WBNP) drag counts at $C_L = 0.5$ (Fig. 3). In general the drag prediction of the present study is somewhat worse than that of codes more specialized in aeronautical applications than the one used here.

The change of drag due to the nacelle and pylon interactions can be expressed through the notion of installation drag, which includes the external drag of the nacelles, the drag of the pylons, and the interference drag, and is defined as follows:

$$\Delta C_{D\,\text{inst}} = C_{D,\,\text{WBPN}} - C_{D,\,\text{WB}} \tag{1}$$

For example, at $C_L = 0.5$ the drag coefficient increment was measured at 0.0043 [12,16] while the predicted value in the present study was 0.0039.

Plots of the spanwise lift distribution clearly show that the installation of the nacelle and pylon has a significant effect on the local lift (Fig. 4) and in turn on the wing loading distribution and, by implication, on the induced drag of the wing. The kink in the local lift distribution is traceable to a separation on the inboard side of the pylon ($Y_{\text{pylon}}/S = 0.355$), which was also observed in experimental flow visualizations [8].

Overall, CFD methods have the potential of predicting changes in lift and drag for different design cases, whereas absolute predictions of lift and drag are still questionable. Physically, there is a potential for drag reduction by careful streamlining the nacelle geometry and the pylon. This is the background of the following study focusing on the effect of changing the pylon to a compression design.

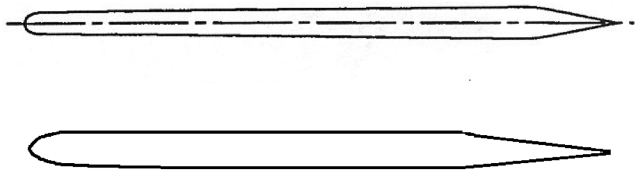

Fig. 1 Compression pylon shape (top) [9] and conventional pylon shape (DLR F6).

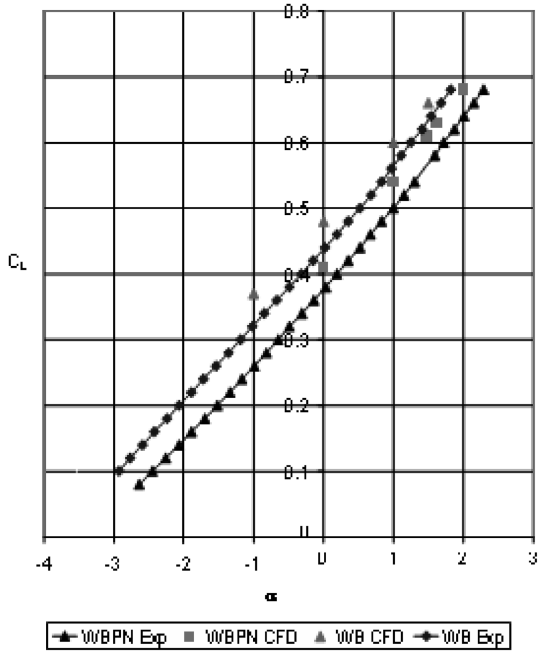

Fig. 2 Lift coefficient vs angle of attack.

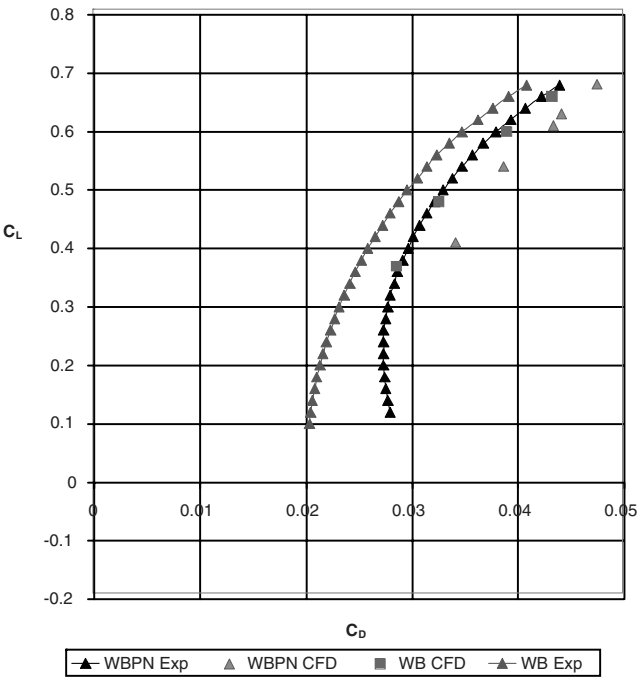

Fig. 3 Lift coefficient vs drag coefficient.

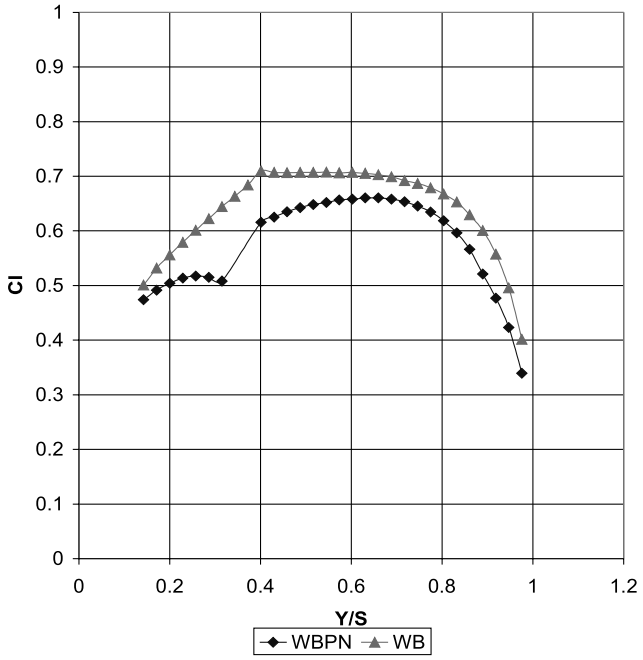

Fig. 4 Spanwise local lift coefficient.

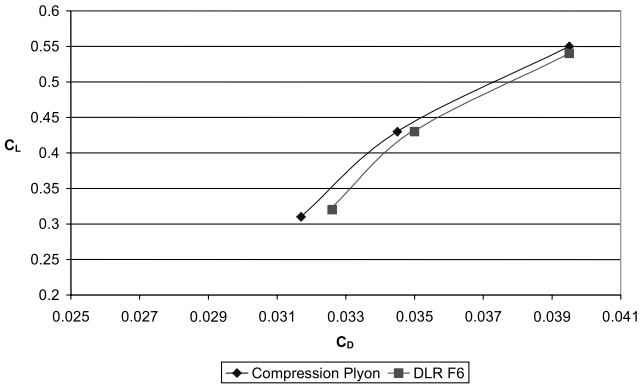

Fig. 5 Lift vs drag of baseline case to compression pylon case.

When a change of pylon to compression type is considered, at three angles of incidence, −1, 0, and 1 deg, the compression pylon produces slight reductions in drag associated with small variations of lift (Fig. 5). At zero incidence, the lift and drag coefficients for the compression pylon were 0.432 and 0.03456, respectively, compared to the corresponding values for the conventional pylon of 0.426 and 0.03498, respectively. For the same lift coefficient, the compression pylon produced a drag reduction of approximately 0.0006.

The origin of these changes can be traced in the comparison of pressure distributions for the baseline case and compression pylon case (Fig. 6). The pressure distributions on the inboard of the pylon indicate the presence of a shock wave on the lower surface in both cases, but the shock wave position in the compression pylon case is farther downstream than that of the baseline case. As a consequence the shock strength in the compression pylon case is slightly stronger. However, farther downstream of the shock the pressure recovery for the compression pylon produces increased lift from the lower surface of the wing. Although some changes are noted on the lower surface, both the upper surface and the outboard of the pylon pressure patterns are relatively unchanged.

The change of geometry to a compression pylon also reduces the interference effects on the spanwise lift coefficient distribution in the outboard region thus indicating the aerodynamic integration of the wing, pylon, and nacelle needs to focus on the inboard geometry.

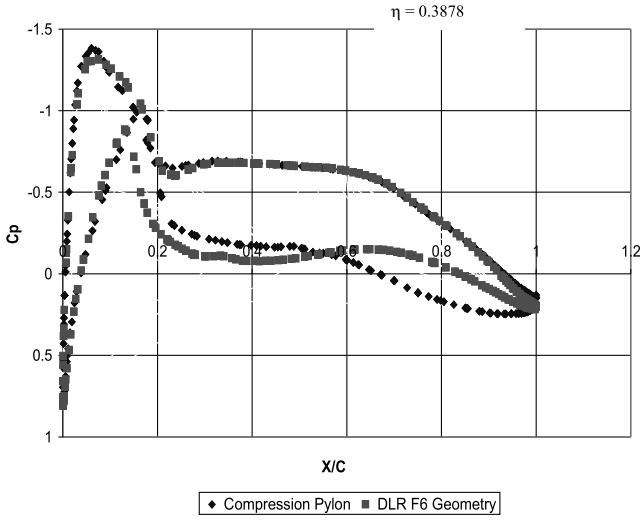

Fig. 6 Wing pressure coefficient in the inboard neighborhood of the nacelle.

V. Conclusions

The results of a computational investigation comparing the aerodynamic performance of a compression pylon design to a DLR F6 based conventional pylon design are presented in this paper. As with other computational predictions, the total lift and total drag were overpredicted. The change in drag between the wing body and the wing-body nacelle-pylon configurations was underpredicted by 14% at $C_L = 0.5$. This validated CFD method was then used to investigate a compression pylon design. The results showed that a compression pylon produces an increase in lift and a reduction in drag. At zero degree angle of attack the total drag coefficient was reduced by at least 0.0006. The effect of the pylon is primarily inboard of the wing. These results demonstrate the need to consider the inboard geometry of the wing, pylon, and nacelle when the aerodynamic integration of a powerplant is being considered. This type of consideration will especially be of importance when laminar flow nacelles are designed.

Acknowledgments

The authors wish to thank Invest NI, Bombardier, and the Royal Academy for their financial support for these investigations.

References

[1] Berry, D., "The Boeing 777 Engine/Airframe Integration Aerodynamics Design Process," *Proceedings of the International Council of the Aeronautical Sciences*, AIAA, Washington, D.C., Sept. 1994, 94–6.4.4, ISBN-13: 978-1563470844.

[2] Carlson, J. R., and Lamb, M., "Integration Effects of Pylon Geometry on a High-Wing Transport Airplane," NASA TP 2877, 1989.

[3] Ingraldi, A. M., Kariya, T. T., Re, R. J., and Pendergraft, O. C., "Interference Effects of Very High Bypass Ratio Nacelle Installations on a Low-Wing Transport," *Journal of Engineering for Gas Turbines and Power*, Vol. 114, No. 4, Oct. 1992, pp. 809–815. doi:10.1115/1.2906661

[4] Riedel, H., Horstmann, K. H., Ronzheimer, A., and Sitzmann, M., "Aerodynamic Design of a Natural laminar Flow Nacelle and the Design Validation by Flight Testing," *Aerospace Science and Technology*, Vol. 2, No. 1, 1998, pp. 1–12. doi:10.1016/S0034-1223(98)80001-8

[5] Godard, J. L., Hoheisel, H., Rossow, C. C., and Schmitt, V., "Investigation of Interference Effects for Different Engine Positions on a Transport Aircraft Configuration," *Proceedings of the DLR Workshop on Aspects of Engine Airframe Integration for Transport Aircraft*, edited by H. Hoheisel, German Aerospace Research Centre, DLR, Brunswick, Germany, 1996, TR 96-01, pp. 11.1–11.22.

[6] Henderson, W. P., "Airframe/Propulsion Integration at Transonic Speeds," *Journal of Engineering for Gas Turbines and Power*, Vol. 113, No. 1, Jan. 1991, pp. 51–59. doi:10.1115/1.2906530

[7] Ingraldi, A. M., Kariya, T. T., Re, R. J., and Pendergraft, O. C., "Interference Effects of Very High Bypass Ratio Nacelle Installations on a Low-Wing Transport," *Journal of Engineering for Gas Turbines and Power*, Vol. 114, No. 4, Oct. 1992, pp. 809–815. doi:10.1115/1.2906661

[8] Rudnik, R., and Rossow, C. C., "Numerical Simulations of Engine/Airframe Integration for High-Bypass Engines," *Book of Abstracts of ECCOMAS—2000 Barcelona*, Publisher, Location, 2000, 11.-14.09, ISBN 84-89925-69-0.

[9] Carlson, J. R., and Lamb, M., "Integration Effects of Pylon Geometry on a High-Wing Transport Airplane," NASA TP 2877, 1989.

[10] Rudnik, R., Rossow, C. C., and v. Geyr, H. F., "Numerical Simulation of Engine/Airframe Integration for High-Bypass Engines," *Aerospace Science and Technology*, Vol. 6, No. 1, 2002, pp. 31–42. doi:10.1016/S1270-9638(01)01139-7

[11] Mavriplis, D. J., "Drag Prediction Using Unstructured Mesh Solvers," *CFD-Based Aircraft Drag Prediction and Reduction*, VKI Lecture Notes, Von Karman Institute for Fluid Dynamics, Rhode-Saint-Genese, Belgium, Feb. 2003.

[12] Laflin, K. R., Klausmeyer, S. M., Zickuhr, T., Vassberg, J. C., Wahls, R. A., Morrison, J. H., Brodersen, O., Rakowitz, M., Tinoco, E. N., and Godard, J-L., "Data Summary from Second AIAA Computational Fluid Dynamics Drag Prediction Workshop," *Journal of Aircraft*, Vol. 42, No. 5, Sept.–Oct. 2005, pp. 1165–1178. doi:10.2514/1.10771

[13] Rossow, C. C., Godard, J.-L., Hoheisel, H., and Schmitt, V., "Investigation of Propulsion Integration Interference Effects on a Transport Aircraft Configuration," *Journal of Aircraft*, Vol. 31, No. 5, 1994, pp. 1022–1030. doi:10.2514/3.46605

[14] Rumsey, C. L., Rivers, S. M., and Morrison, J. H., "Study of CFD Validation on Transport Configurations," AIAA Paper 2004-0394, 2004.

[15] Lee-Rausch, E., Fink, N. T., Milholen, W. E., and Mavriplis, W. E., "Transonic Drag Predictions Using Unstructured Grid Solvers," AIAA Paper 2004-0554, Jan. 2004.

[16] Brodersen, O., "Drag Prediction of Engine-Airframe Interference Effects Using Unstructured Navier-Stokes Calculations," *Journal of Aircraft*, Vol. 39, No. 6, 2002, pp. 927–935. doi:10.2514/2.3037

[17] Rossow, C. C., and Hoheisel, H., "Numerical Studies of Interference Effects of Wing-Mounted Advanced Engine Concepts," International Council of the Aeronautical Sciences (ICAS) Paper 94-6.4.1, Sept. 1994.